Preprints of the 21st IFAC World Congress (Virtual)
Berlin, Germany, July 12-17, 2020

Flow monitoring for continuous steel casting using Contactless Inductive Flow Tomography (CIFT)

I. Glavinić *, **M. Ratajczak**, **F. Stefani**, **T. Wondrak**

* *Helmholtz-Zentrum Dresden-Rossendorf, Bautzner Landstraße 400, 01328 Dresden - Germany (e-mail: i.glavinic@hzdr.de).*

Abstract: The control of the liquid steel flow in the mould of a continuous caster based on real time flow measurements is a challenging task due to the lack of appropriate measurement techniques. The opaqueness, the high temperature of 1500°C and the chemical aggressiveness of the melt require non-optical contactless methods. In order to reconstruct the complex flow structure in the mould, the Contactless Inductive Flow Tomography (CIFT) is a promising candidate, since it allows the visualization of the flow structure in the melt by applying a magnetic field to the melt, measuring the flow induced perturbation of that field and solving subsequently a linear inverse problem. The combination of this new measurement technique with typical electromagnetic actuators like electromagnetic brakes used in continuous casting pose a challenge to the CIFT measurement system, because the flow induced magnetic field is in the range of 100 nT and has to be measured robustly on the background of the static magnetic field with the amplitude of 300 mT generated by the brake. In this work we will show recent developments regarding this topic for a small model of a continuous caster in the lab. Furthermore, we will present a new method on how the complex linear inverse problem can be solved in real time providing a time resolution of about 1 Hz.

Keywords: Tomography-based industrial process control, CIFT, Continuous casting, mini-LIMMCAST, Process tomography sensors

1. INTRODUCTION

Continuous casting is the most used technique for steel production in the world. Figure 1 shows a schematic of a continuous caster. The liquid steel is transported to the continuous caster by large ladles and poured into the tundish, which serves as buffer storage during changing of ladles. From the tundish the liquid steel flows continuously through the submerged entry nozzle (SEN) into the water cooled mould, where the liquid steel starts to solidify on the copper walls. The flow rate of liquid metal is controlled by a stopper rod or a sliding gate at the SEN. In order to avoid clogging of the SEN and to catch non-metallic inclusions in the liquid, sometimes argon gas is injected via the tip of the stopper rod or a porous region at the SEN. The free surface of the liquid steel in the mould is covered by slag and flux powder for thermal shielding. The partly solidified strand with a liquid core leaves the bottom of the mould and is transported by a set of motor driven rolls, while it is sprayed with cooling water to accelerate the solidification (Thomas, 2001). This method enables continuous and steady production of steel. The shape of the mould is usually adapted to the subsequent process chain. While there are moulds for round blooms, billets and beam blanks, only slab casting is investigated in this paper.

The flow regime of the liquid steel in the upper part of the mould has an important impact on the quality of the steel, since conditions during initial solidification of

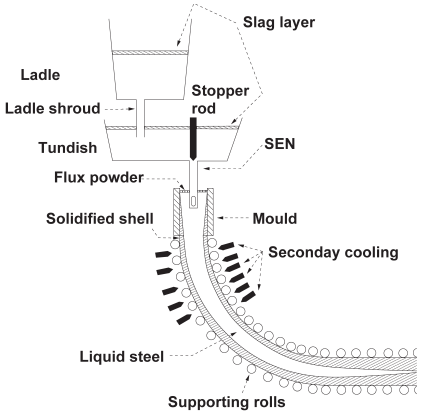

Fig. 1. Schematic of a continuous caster

steel in the mould are crucial for successful production, and substantially influence the quality of the end product (Dauby, 2012). In literature, three different flow regimes are distinguished, two of which are depicted in Figure 2. Important parameters are the position of the impingement of jets leaving the ports of the SEN and the velocity at the free surface of the liquid steel. The velocity at the meniscus has to be kept in a certain interval, since for too low velocities the risk of meniscus freezing is increased, while for too high velocities the slag on the meniscus may be entrained into the liquid steel (Zhang et al., 2007). The impingement position of the jet should also be kept in a certain range, since too deep positions prevent the

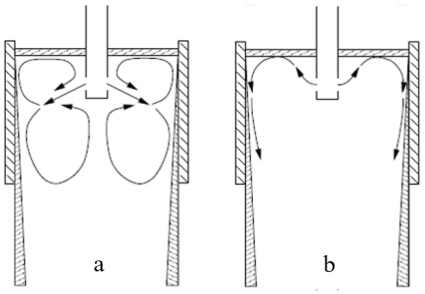

Fig. 2. Mould and SEN with double-roll flow (a), and single-roll flow (b)

floating of argon bubbles, as well as non-metallic inclusions to the meniscus, while too shallow positions increase the velocity at the meniscus. Furthermore, asymmetric flows, as they may result from uneven discharge from opposite ports of the SEN, can lead to undesirable oscillations of the meniscus. Taking these considerations into account, the best flow regime is a stable double-roll flow structure, as seen in Figure 2(a). In contrast, a single-roll flow, as depicted in Figure 2(b), can occur for too high argon flow rates. The direct impingement of the jet at the meniscus leads to slag entrainment. It is obvious that constant observation of the process is desired.

In order to optimize and control the flow during a casting sequence, electromagnetic actuators are used, which allow to influence the flow using Lorentz forces. They can be divided into Electromagnetic Brakes (EMBr) and Electromagnetic Stirrers (EMS). Electromagnetic brakes generate a static magnetic field which is often applied in the region below the ports of the SEN. Electromagnetic stirrers, on the other hand, generate a rotating or a travelling magnetic field and, depending on its movement, the liquid steel is accelerated or decelerated. A detailed overview of electromagnetic actuators used in continuous steel casting can be found in the recent publication by Cho and Thomas (2019).

The control of the electromagnetic actuators during the process based on the actual flow regime in the mould would be highly desirable, in order to be able to react accordingly on flow instabilities in the mould. However, the high temperature, the chemical aggressiveness and the opaqueness of liquid steel set high demands on a measurement system. One promising candidate for such measurement technique is the Contactless Inductive Flow Tomography (CIFT) which is able to reconstruct the three-dimensional flow structure in liquid metals (Stefani et al., 2004). The working principle relies on the measurement of the flow-induced perturbations of an externally applied magnetic field. From this measurement, the two-dimensional flow structure in the mould is reconstructed by solving a linear inverse problem. In case of a slab casting mould, CIFT was able to reconstruct the dominating two-dimensional flow structure parallel to the wide faces of the mould of a small scale model (1:8) (Wondrak et al., 2010). The measurement system consists of one excitation coil around the mould generating a magnetic field in vertical direction of 1 mT and seven sensors along each narrow face of the mould. In all experiments the reconstructed flow was in reasonable agreement with independent measurements using ultrasonic Doppler velocimetry. Measurements at a larger model of a slab caster (1:2) showed similar results, and thus scaling of the measurement system to larger moulds seems to be feasible (Ratajczak et al., 2015b).

The challenge of CIFT is the robust measurement of the flow induced perturbation of the applied magnetic field, which, for this application, is typically four orders of magnitude lower than the applied magnetic field. In the first experiments, a static excitation magnetic field was used and the magnetic field was recorded by Fluxgate probes with a dynamic range of six orders of magnitude. However, these measurements were extremely sensitive to external interference (Ratajczak et al., 2015). Using an alternating excitation magnetic field allows the actual induced magnetic field to be separated from the environmental noise, suppressing undesired signals from the environment. By this more robust measurement technique, CIFT measurements were realizable even in the presence of a static magnetic field in the order 300 mT generated by an EMBr (Ratajczak et al., 2015a, 2016). Since the effect of the ferromagnetic parts of the brake on the flow induced magnetic field in the present configuration is negligible, the inverse problem remains linear. In order to use CIFT for monitoring the flow in the mould in the presence of an EMBr and providing real-time flow reconstructions to a controller, the following two key issues have to be solved.

First, the effects of changes of the magnetic field of the EMBr on the CIFT measurement system has to be evaluated and compensated. Preliminary results of a potential compensation method will be presented in section 4. Second, the reconstruction algorithm has to be accelerated so that one reconstruction takes less than a second, without reducing the quality of the reconstruction. A proof-of-concept will be delineated in section 5. However, to introduce CIFT and the experiments in more detail, in section 2 we give a mathematical formulation of CIFT, and in section 3 a description of the model of a continuous caster.

2. CONTACTLESS INDUCTIVE FLOW TOMOGRAPHY (CIFT)

The flow reconstruction with CIFT relies on the inversion of the following linearised integral equation system:

$$\boldsymbol{b}(\boldsymbol{r}) = \frac{\mu_0\sigma}{4\pi}\iiint_V \frac{(\boldsymbol{v}(\boldsymbol{r}\,')\times\boldsymbol{B}_0(\boldsymbol{r}\,'))\times(\boldsymbol{r}-\boldsymbol{r}\,')}{|\boldsymbol{r}-\boldsymbol{r}\,'|^3}dV' - \frac{\mu_0\sigma}{4\pi}\oiint_S \frac{\varphi(\boldsymbol{r}\,')\boldsymbol{n}(\boldsymbol{r}\,')\times(\boldsymbol{r}-\boldsymbol{r}\,')}{|\boldsymbol{r}-\boldsymbol{r}\,'|^3}dS' \,, \tag{1}$$

$$\varphi(\boldsymbol{r}) = \frac{1}{4\pi p(\boldsymbol{r})}\iiint_V \frac{(\boldsymbol{v}(\boldsymbol{r}\,')\times\boldsymbol{B}_0(\boldsymbol{r}\,'))\cdot(\boldsymbol{r}-\boldsymbol{r}\,')}{|\boldsymbol{r}-\boldsymbol{r}\,'|^3}dV' - \frac{1}{4\pi p(\boldsymbol{r})}\oiint_S \frac{\varphi(\boldsymbol{r}\,')\boldsymbol{n}(\boldsymbol{r}\,')\cdot(\boldsymbol{r}-\boldsymbol{r}\,')}{|\boldsymbol{r}-\boldsymbol{r}\,'|^3}dS' \,, \tag{2}$$

which enables the computation of the flow induced field $\boldsymbol{b}(\boldsymbol{r})$ outside the volume V of the fluid under the influence of a primary field $\boldsymbol{B}_0(\boldsymbol{r}\,')$, and under the assumptions that the boundary $S = \partial V$ is insulating and the conductivity σ of the liquid is homogeneous (Stefani et al., 2004). Here, φ

denotes the electric scalar potential and $\boldsymbol{v}(\boldsymbol{r}')$ the velocity of the liquid. $p(\boldsymbol{r})$ is a factor with $0 < p < 1$ and is determined by the shape of the boundary surface and depends on the solid angle at the position $\boldsymbol{r}$. A detailed consideration of the singularities in the integral equations and the derivation of p is given in (Jacobs et al., 2018). $\boldsymbol{r}$ and $\boldsymbol{r}'$ are vectors in the 3-D Euclidian space ($\boldsymbol{r}$, $\boldsymbol{r}' \in \mathbb{R}^3$). The integral equations are solved numerically by discretising the volume that contains the liquid and by employing linear shape functions on the resulting surface and volume elements. For a given number of sensors, this leads to a system of linear equations of the form

$$\tilde{b} = M \cdot \tilde{v} \ , \tag{3}$$

where $M = M(\boldsymbol{B}_0)$ is the system matrix and the magnetic flux density $\tilde{b} = \tilde{b}(\boldsymbol{B}_0)$ at the sensors is dependent on the excitation field $\boldsymbol{B}_0$. The vector $\tilde{v}$ denotes the velocity field in the discretised volume.

While for the full three-dimensional reconstruction of the flow two differently directed primary magnetic fields are needed, for the reconstruction of the dominating two-dimensional flow structure in the mould it is sufficient to use only one applied magnetic field (Wondrak et al., 2010). In the present configuration, the primary field $\boldsymbol{B}_0$ is generated by two coils around the mould producing a magnetic field in vertical direction (see section 3). The recorded flow induced magnetic flux density at the sensors is stored as $\tilde{b}(\boldsymbol{B}_0)$. In order to reconstruct the velocity $\tilde{v}$ in the volume, the system of linear equations (see Eq. (3)) needs to be inverted by means of least squares, which amounts to solving the corresponding system of normal equations. Exploiting the incompressibility of liquid melts by allowing only solenoidal velocity fields, and using Tikhonov regularisation to mitigate the intrinsic non-uniqueness of the problem leads to the following residuum to be minimised:

$$\begin{aligned} \min_{\tilde{v}} \Big(& \left\| M(\boldsymbol{B}_0) \cdot \tilde{v} - \tilde{b}(\boldsymbol{B}_0) \right\|_2^2 + \\ & \lambda \left\| G\tilde{v} \right\|_2^2 + \lambda_D \left\| \nabla \cdot \tilde{v} \right\|_2^2 + \\ & \lambda_{2D} \left\| \tilde{v}_y \right\|_2^2 + \lambda_I \left\| C\tilde{v} - \tilde{v}_{inlet} \right\|_2^2 \Big) , \end{aligned} \tag{4}$$

where λ represents the regularisation parameter. This parameter reflects the trade-off between minimising the residual deviation of the measured field and minimising the kinetic energy of the estimated velocity field. λ is determined by the L-curve method (Stefani et al., 2004) using a search algorithm similar to the one described in (Wondrak et al., 2009), which requires approximately 10-30 iterations for the present configuration. The second parameter λ_D is chosen rather large to ensure the divergence-free condition of the reconstructed velocity. The last two terms enforce the velocity to be two dimensional by setting the component v_y (normal to the wide face of the mould) to zero, and provide the mean velocity $\tilde{v}_{inlet}$ at the inlet of the SEN. Both parameters λ_{2D} and λ_I are chosen rather large.

3. EXPERIMENTAL SETUP

The basis for the experiments is a small model of a continuous caster consisting of a tundish, SEN and mould made out of acrylic glass (Timmel et al., 2010; Schurmann et al., 2019). A schematic representation of the liquid metal loop of this facility, called *Mini-LIMMCAST*, is depicted in Figure 3.

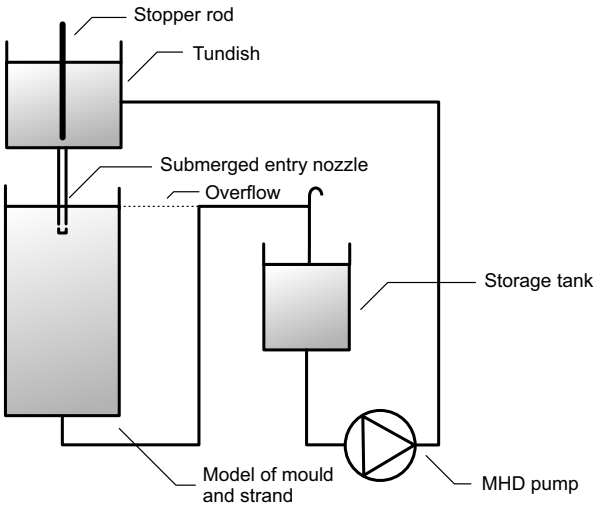

Fig. 3. Schematic representation of the liquid metal loop.

It is operated with an eutectic alloy Gallium-Indium-Tin (GaInSn) which is non-toxic, and liquid at room temperature. The mould has a cross-section of 300×35 mm and a height of 600 mm. The SEN has an inner diameter of 12 mm with two side ports directed downward at an angle of 15°. The facility is operated in continuous mode, allowing for experimental runs over several hours. The liquid metal is pumped from the storage tank into the tundish above the mould, from where it flows through the SEN into the mould. The flow rate is regulated by changing the position of the stopper rod. The liquid leaves the mould at the bottom and flows back into the storage tank. The vertical position of the overflow determines the level of the free surface in the mould.

Mini-LIMMCAST can be equipped with an electromagnetic brake that generates a static magnetic field at a defined vertical position along the entire width of the mould. It consists of two water cooled coils connected in series, rated for maximum current of 600 A generating maximum strength of magnetic field of 406 mT. A more detailed description of the Mini-LIMMCAST facility and its comparison to industrial casters is given by Schurmann et al. (2019).

The excitation magnetic field for CIFT is generated by two coils around the mould, positioned above and below the poles of the brake, as seen in Figure 4. The two coils jointly generate an alternating magnetic field of approx. 1.55 mT in the vertical direction at the centre with a rather low frequency in the order of 1 Hz to avoid the skin effect which would prevent the applied magnetic field from penetrating the entire volume of liquid metal. To measure the flow induced magnetic field, seven induction coils are placed along each narrow face of the mould. The coils are arranged in a vertical array and tightly fixed to the excitation coils as well as to the EMBr.

The induction coils without ferromagnetic cores have the advantages that they have a perfectly linear response of

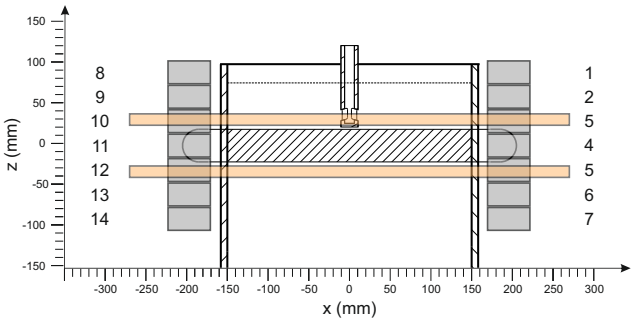

Fig. 4. Schematic representation of CIFT assembly with the two excitation coils (orange) and 2×7 pickup induction coils along the narrow faces of the mould.

induced voltage to applied magnetic field at a given frequency, have no upper range limit in amplitude of the magnetic field, and are not sensitive to static magnetic fields. The use of an alternating applied magnetic field allows the flow induced magnetic field to be locked-on and separated from the environmental noise. Two different kinds of coils are used: absolute and gradiometric induction coils. Absolute sensors consist of a single coil and detect the absolute value of the magnetic field, whereas gradiometric sensors comprise two coils, wound in opposing directions and then connected in series, rejecting magnetic fields that are uniform along the axis of sensor (Ratajczak et al., 2016; Ratajczak and Wondrak, 2020).

4. EFFECT OF THE EMBR ON THE EXCITATION FIELD

A key challenge of applying CIFT in continuous casting with EMBr is the presence of the large ferromagnetic pole shoes of the brake, which amplify the magnetic field of the brake. These parts also have an effect on the excitation, as well as on the flow induced magnetic field. Numerical calculations suggest that the effect on the flow induced magnetic field is negligible in the present configuration so that the integral equation system given in equation (1) and (2) has not to be changed. However, the effect on the excitation magnetic field is huge (Ratajczak et al., 2015a), demanding two excitation coils, above and below the pole shoes of the brake, in order to penetrate the entire mould with the excitation magnetic field. For the reconstruction, the applied magnetic field $\boldsymbol{B}_0$ generated by the two coils has to be simulated using a finite element method, which takes the ferromagnetic parts into account.

For the sake of simplicity, the previous measurements with CIFT were conducted without changing the strength of the brake during the measurement. It could be shown that with a moderately high excitation frequency of 8 Hz, the key flow features could be reconstructed (Ratajczak et al., 2016). However, for controlling the flow using EMBr with CIFT in a feedback loop, the strength of magnetic field of EMBr has to be readjusted accordingly, so these effects now have to be carefully considered. In the first step we simulated and measured the magnetic field generated by the two excitation coils for CIFT with an excitation current of 25 A and a frequency of 1 Hz, while the brake

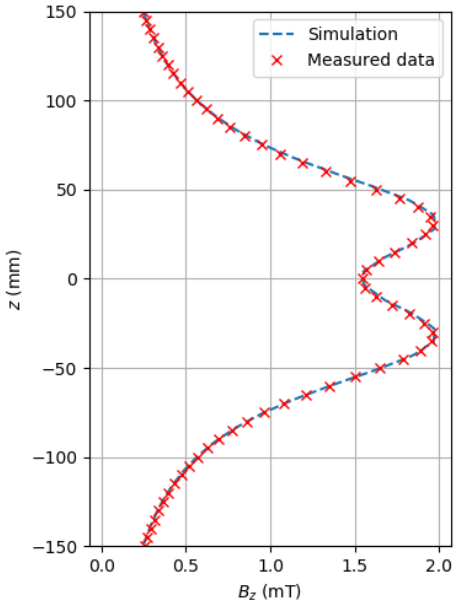

Fig. 5. Simulation and measurement of excitation magnetic field along the z axis at $x = 0$ and $y = 0$

was switched off. The magnetic field was measured along the vertical centre line of the mould with a 3-axis Hall effect probe of a *Lake Shore's Model 460*. The probe was mounted to a 3-axis positioning device. Figure 5 shows the comparison of the simulation and the measurement of the magnitude of the magnetic field.

Additionally, the excitation magnetic field was measured along the vertical line, where the CIFT sensors will be positioned, for different strengths of the EMBr. Figure 6 shows the changes of the horizontal and vertical component of the excitation magnetic field for CIFT, if the brake was operated with 50, 100, 300 and 600 A. For the highest current of the brake, the changes are two orders of magnitude lower than the applied magnetic field. It is interesting to note that the amplitude of the horizontal component of magnetic field decreases while the vertical component of magnetic field increases, if the strength of the brake rises.

In order to investigate the influence of the brake on the CIFT measurement system further, we assembled the system with 14 gradiometric coils, seven on each side of the mould, with the axis of coils perpendicular to the narrow side of the mould (Figure 4). We change the strength of the magnetic field of EMBr, and observe its influence on the value of the flow induced magnetic field. We quantify this effect by varying the strength of the EMBr without the flow of the liquid metal.

Figure 7 shows the result matrix for one series of measurements for the sensor 11, where the current of the EMBr was changed from 0 A to 600 A and back to 0A, in steps of 50 A. It depicts the mean value of the change of the flow induced magnetic field as a result of varying the strength of the EMBr. Current before the change is labelled on y-axis, and current after the change is labelled on x-axis. The colour represents the standard deviation of the change of flow induced magnetic field for three consecutive

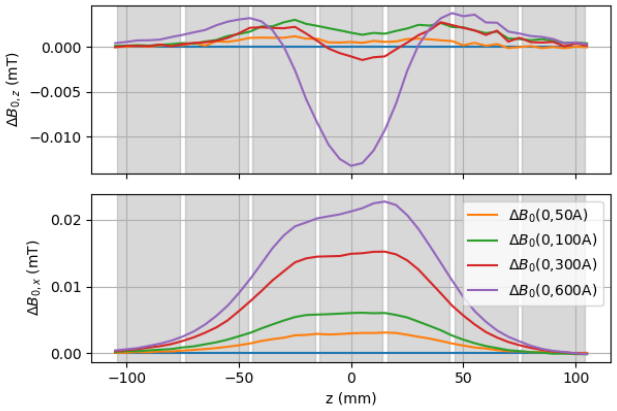

Fig. 6. Difference of the x and z component of the excitation magnetic field along the narrow faces of the mould at the position of the sensors ($x = 185\ mm$, $y = 0\ mm$) for different currents of the brake. Grey area represents the position of seven gradiometric coils. Measurements were done using Hall probe with position resolution of $5\,mm$.

measurements, and the shown value is the mean value of the change. Sensor 11 was selected as it had the most pronounced standard deviation, other sensors have less. We noticed that the majority of the deviation is a result of the first repetition of the current scheme, the difference between mean values of change for the second and third repetition are much lower. Similar results were observed when we chose a different current scheme for the EMBr. However, it is worth noticing that the mean change of inphase value depends on whether the current is rising or falling which comes from the fact that the ferromagnetic material of the EMBr exhibits phenomenon of magnetic hysteresis. In order to compensate the effects of the EMBr on the measurement, a model will be developed which corrects the measured flow induced magnetic field.

5. REAL TIME RECONSTRUCTION

When CIFT is used as a monitoring system for a control loop, the reconstruction of the flow in the mould has do be completed in the time frame of a measurement cycle, i.e. in less than 1 s. The presently used direct method relies on the solution of the normal equations

$$A_\lambda^T A_\lambda \tilde{v} = A_\lambda^T \tilde{b}\ , \tag{5}$$

where the matrix $A \in \mathbb{R}^{n\times 3m}$ is given by the argument of equation (4) and depends on the regularisation parameter λ. The matrix A_λ^T denotes the transpose of A_λ. The parameter n represents the number of sensors, which is equal to 14 in the present setup for continuous casing (see. Fig. 4). The parameter m is the number of points in discretised volume V, where each point is associated with three components of the vector field. For the present reconstruction m equals to 9918. For Tikhonov regularisation, equation 5 needs to be evaluated for various values of λ to determine the parameter value that leads to the best approximation. The direct method solves equation (5) for each value of λ by Cholesky decomposition, of which the operation count is of $\mathcal{O}((3m)^3)$. A significant acceleration of the inversion could be achieved, if the matrix $\tilde{A}_\lambda \in \mathbb{R}^{3m\times n}$ defined by

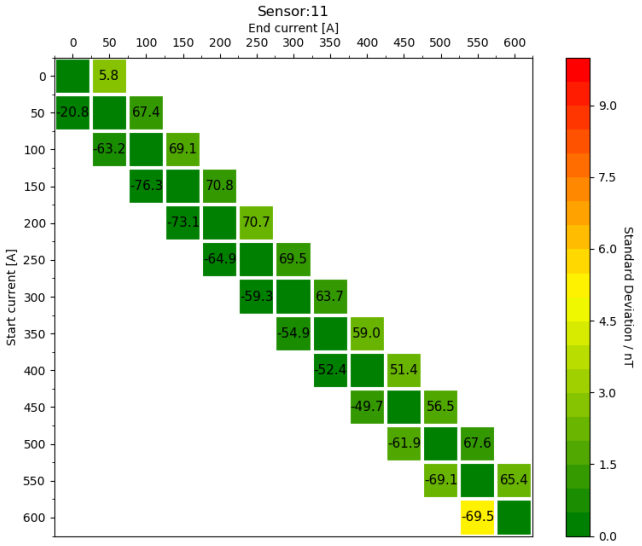

Fig. 7. Difference of measured mean value of flow induced magnetic field for transition from one current value (y-axis) of EMBr to another value (x-axis), colour scale shows a standard deviation of difference for each current pair of three consecutive measurements.

$$\tilde{A}_\lambda = (A_\lambda^T A_\lambda)^{-1} A_\lambda^T \tag{6}$$

is computed before the measurement. Then, only a matrix-vector multiplication with $3mn$ numerical operations is needed. For the fast reconstruction method, the matrix $\tilde{A}_\lambda$ is computed for a list of l different regularisation parameters. In this case the reconstruction needs only l matrix-vector multiplications instead of l Cholesky decompositions. Examining the large number of reconstructions from the two-phase experiments described in Wondrak et al. (2011), it turned out that the best regularisation parameter changes only in a very limited interval and that the dependence of the reconstructed velocity field from the regularisation parameter is very smooth so that a small deviation from the best regularisation parameter diminishes the reconstruction quality only slightly (Ratajczak et al., 2016). Therefore, it is expected that a moderate number of pre-computed matrices is sufficient. In order to compare the run-time of the direct method with the fast method, both procedures were implemented in the programming language Python using the libraries NumPy and OpenBLAS. The experiments were conducted on an Intel i7-2600 processor with 4 cores and 16 GB RAM. The direct method solved equation (5) 15 times using Cholesky decomposition in 739 seconds. In contrast, the fast method utilising the 15 pre-computed matrices according to equation (6) needed only 0.1s. The difference between both reconstructed velocities is negligible.

Figure 8 shows the reconstruction of the flow in the upper part of the mould using a time averaged magnetic field measurement from Mini-LIMMCAST, where the stopper rod was opened 5 mm and the EMBr was not mounted to the mould. The typical impingement position of the jet at the narrow faces of the mould is clearly detectable. A comprehensive study about the numerical stability, the number of required pre-computed matrices and about the acceleration with GPUs is on the way.

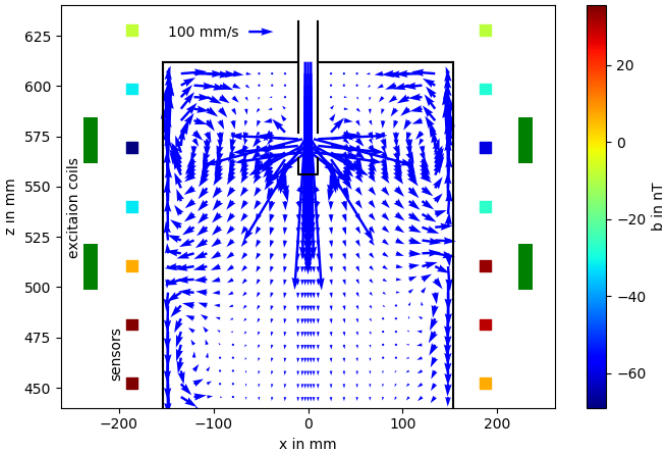

Fig. 8. Reconstructed flow and the measured induced magnetic field at the sensors outside the mould without the EMBr.

6. CONCLUSION

A flow monitoring system for the mould of a continuous steel caster would be highly desirable. In model experiments with a small mould (1:8) the dominating two-dimensional flow structure could be reconstructed even in the presence of an electromagnetic brake. In order to extend CIFT to a monitoring system, which can be used as a sensor for a control loop, a real-time reconstruction algorithm was developed. It could be shown that the reconstruction can be executed in less than one second, still using the L-curve method to select the best regularisation parameter. Furthermore, preliminary measurements indicate that the influence of the strength of the electromagnetic brake on the CIFT measurements could be compensated. Therefore, CIFT might be able to act as a flow sensor for a control loop for continuous casting. First attempts to develop a control loop based on the flow regime in the mould were investigated by Abouelazayem et al. (2019).

ACKNOWLEDGEMENTS

This project has received funding from the European Union's Horizon 2020 research and innovation programme under the Marie Sklodowska-Curie grant agreement No 764902 (TOMOCON - www.tomocon.eu).

REFERENCES

Abouelazayem, S., Glavinić, I., Wondrak, T., and Hlava, J. (2019). Control of jet flow angle in continuous casting process using an electromagnetic brake. In *IFAC-PapersOnLine*, volume 52, 88–93.

Cho, S.M. and Thomas, B.G. (2019). Electromagnetic forces in continuous casting of steel slabs. *Metals*, 219(9), 471.

Dauby, P. (2012). Continuous casting: Make better steel and more of it. *Revue de Métallurgie*, 109, 113–136.

Jacobs, R., Wondrak, T., and Stefani, F. (2018). Singularity consideration in the integral equations for contactless inductive flow tomography. *COMPEL*, 37(4), 1366–1375.

Ratajczak, M., Wondrak, T., Stefani, F., and Eckert, S. (2015a). Numerical and experimental investigation of the contactless inductive flow tomography in the presence of strong static magnetic fields. *Magnetohydrodynamics*, 51, 461–471.

Ratajczak, M., Wondrak, T., Timmel, K., Stefani, F., and Eckert, S. (2015b). Flow visualization by means of contactless inductive flow tomography in the presence of a magnetic brake. *Journal for Manufacturing Science and Production*, 15, 41–48.

Ratajczak, M., Wondrak, T., Zürner, T., and Stefani, F. (2015). Enhancing robustness and applicability of contactless inductive flow tomography. In *2015 IEEE SENSORS*, 1–4.

Ratajczak, M. and Wondrak, T. (2020). Analysis, design and optimization of compact ultra-high sensitivity coreless induction coil sensors. *Measurement Science and Technology*, 31(6), 065902.

Ratajczak, M., Wondrak, T., and Stefani, F. (2016). A gradiometric version of contactless inductive flow tomography: Theory and first applications. *Philosophical Transactions of the Royal Society A*, 374, 20150330.

Schurmann, D., Glavinić, I., Willers, B., Timmel, K., and Eckert, S. (2019). Impact of the electromagnetic brake position on the flow structure in a slab continuous casting mold: An experimental parameter study. *Metallurgical and Materials Transactions B*.

Stefani, F., Gundrum, T., and Gerbeth, G. (2004). Contactless inductive flow tomography. *Physical Review E*, 70(5), 056306.

Thomas, B. (2001). Continuous casting. In *Encyclopedia of Materials: Science and Technology (Second Edition)*, 1595–1598. Elsevier.

Timmel, K., Eckert, S., Gerbeth, G., Stefani, F., and Wondrak, T. (2010). Experimental modeling of the continuous casting process of steel using low melting point metal alloys; the LIMMCAST program. *ISIJ International*, 50(8), 1134–1141.

Wondrak, T., Eckert, S., Gerbeth, G., Klotsche, K., Stefani, F., Timmel, K., Peyton, A.J., Terzija, N., and Yin, W.L. (2011). Combined electromagnetic tomography for determining two-phase flow characteristics in the submerged entry nozzle and in the mold of a continuous casting model. *Metallurgical and Materials Transactions B*, 42(6), 1201–1210.

Wondrak, T., Galindo, V., Gerbeth, G., Gundrum, T., Stefani, F., and Timmel, K. (2010). Contactless inductive flow tomography for a model of continuous steel casting. *Measurement Science and Technology*, 21, 045402.

Wondrak, T., Stefani, F., Gundrum, T., and Gerbeth, G. (2009). Some methodological improvements of the contactless inductive flow tomography. *International Journal of Applied Electromagnetics and Mechanics*, 30(3-4), 255–264.

Zhang, L.F., Yang, S.B., Cai, K.K., Li, J.Y., Wan, X.G., and Thomas, B.G. (2007). Investigation of fluid flow and steel cleanliness in the continuous casting strand. *Metallurgical and Materials Transactions B*, 38, 63–83.